ACTIVE SONAR FOR OBSTACLE LOCALIZATION USING ENVELOPE SHAPE INFORMATION*

Billur Barshan and Roman Kuc

Intelligent Sensors Laboratory
Department of Electrical Engineering
Yale University
New Haven, CT 06520

Abstract

A sonar system that simulates the sensor configuration of echolocating bats is described. Two estimators for range and azimuth of an obstacle are developed, based on the received signal envelope. The standard threshold detector produces a biased time-of-flight (TOF) estimate. An unbiased TOF estimate is derived by using the echo waveform shape to estimate the object location. The estimates are most accurate if the obstacle is located along the "line-of-sight" and improve with decreasing range.

1 Introduction

Acoustic sensors provide an inexpensive means for determining the proximity of obstacles for robot navigation [1, 2, 3, 4]. Reliable obstacle detection by sonar is achieved by densely scanning the environment [5] which is usually time consuming. We propose an efficient, wide-beam sonar system by mimicking the sensor configuration of bats with a transmitter (the mouth) flanked by two receivers (the ears). The useful information is extracted from the received signal envelope through a parabolic fit method.

2 Description of the Sonar System

The Panasonic piezoelectric transducer is employed both as a transmitter (T) and a receiver (R). In the far-zone of the transducer, the beam forms a divergent cone(Fig. 1) with half beam-width angle $\theta_o = \sin^{-1}[\frac{0.61\lambda}{a}]$, where $\lambda = \frac{c}{f_o}$ and c is the sonic speed. For our system, f_o=40kHz, a=7mm, and θ_o=48°. Previous results [6] indicate that in the far-zone, the pressure amplitude of the propagating pulse at range r and azimuth θ can be approximated as:

$$p(r,\theta) = \frac{c_o}{r}\ \exp\left(-\frac{2\theta^2}{\theta_o^2}\right) \qquad (1)$$

where c_o is the amplitude measured on the beam axis at unity range. For a T/R pair, the product of the two beam patterns determines the echo amplitude:

$$A(r_1, r_2, \theta_1, \theta_2) = \epsilon \frac{c_o^2}{r_1 r_2}\ \exp\left[\frac{-2(\theta_1^2 + \theta_2^2)}{\theta_o^2}\right] \qquad (2)$$

where θ_1 and θ_2 are the angles, and r_1 and r_2 are the distances of the obstacle from T and R respectively, and ϵ is the reflection coefficient of the object.

*This work was supported by the NSF grant ECS-8802627.

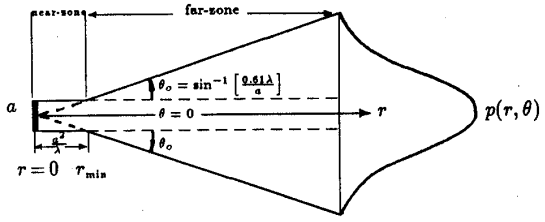

Figure 1. The beam pattern for the Panasonic transducer.

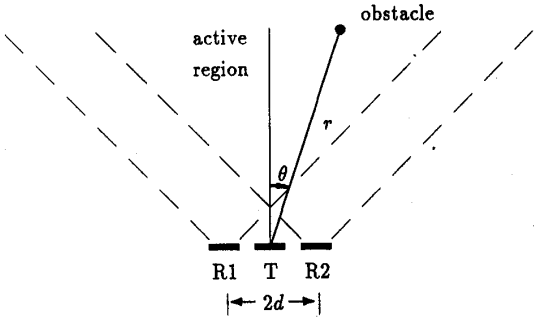

Figure 2. Sonar system configuration.

As illustrated in Fig. 2, T transmits an acoustic pulse, and R1 and R2 capture the echoes. An obstacle is detectable by *both* receivers if it lies in the *active region* of the sonar system, defined by the intersection of the receiver beam patterns. The range r and azimuth θ of an obstacle are measured relative to T.

3 Signal Observation Model

The detected echo is narrowband, with its spectrum evenly spread about f_o, and embedded in additive white Gaussian noise. Envelopes of the noisy echoes are extracted and modeled as follows:

$$s(t) = a_o\ e^{-a_1(t-t_F)}\ (t-t_F)^2\ u(t-t_F) + n(t) \qquad (3)$$

where t_F is the *time-of-flight*. The $u(t-t_F)$ is a unit-step-function delayed by t_F and a_o, a_1 are the parameters of the envelope. In Fig. 3, the form of the noiseless envelope is shown whose maximum value $A(r_1, r_2, \theta_1, \theta_2) = 4a_o(a_1 e)^{-2}$ occurs at $t = t_F + \frac{2}{a_1}$. In our system, the value of a_1 in (3) is sufficiently small so that the exponential term can be

CH2977-7/91/0000-1273 $1.00 © 1991 IEEE

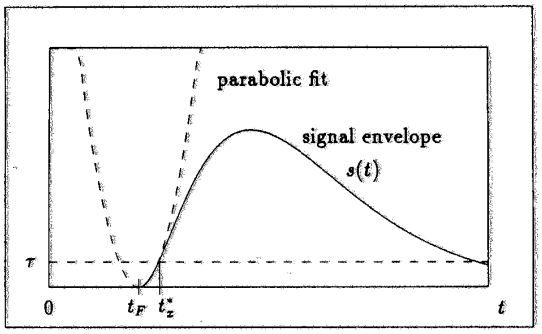

Figure 3. Signal envelope and the parabolic fit.

neglected, and a parabola is a good approximation in the time interval $[t_F,\ t_F + \frac{1}{2a_1}]$. Then, the signal observation model becomes

$$s(t) = a_o(t - t_F)^2 + n(t) \quad \text{for} \quad t \in \left[t_F,\ t_F + \frac{1}{2a_1}\right] \tag{4}$$

Uniform sampling in time produces the sequence:

$$s_k = a_o(t_k - t_F)^2 + n_k \quad \text{for} \quad t_k \in \left[t_F,\ t_F + \frac{1}{2a_1}\right] \tag{5}$$

4 Time-of-Flight Measurement

The range r and azimuth θ of an obstacle need to be estimated from the TOF information, using the envelopes of the noisy echoes detected by the two receivers. Two different methods of estimating the TOF will be compared: $\tilde{t}_F$ from simple thresholding method and $\hat{t}_F$ from the envelope shape information.

4.1 Simple Thresholding Method

The most common method for extracting the TOF information from the echo is simple thresholding [7]. A system threshold τ is set to prevent false obstacle detection due to noise effects. When the signal envelope exceeds τ, the travel time from pulse transmission is measured with resolution T_s. The noiseless signal envelope first crosses the threshold τ at time t_z^* as shown in Fig. 3. Equating the noiseless $s(t)$ in (4) to τ, and solving for t_z^*, we find:

$$t_z^* = t_F + \sqrt{\frac{\tau}{a_o}} \tag{6}$$

However, the time t_z, when the signal *plus* noise first exceeds the threshold need not equal t_z^*. With a discrete system, the TOF estimate is equal to $\tilde{t}_F = k_F T_s = t_z + \Delta$ where Δ is a random delay uniformly distributed in $[0, T_s)$.

Statistics for this estimator need to be derived to evaluate the bias and the variance of $\tilde{t}_F$. Suppose that the parameters a_o and t_F are known. When $t_k \le t_F$, s_k is a normally distributed random variable with mean ξ and variance σ_n^2. The mean ξ emerges due to the envelope detection of noise when no signal is present. If $t_k > t_F$, the

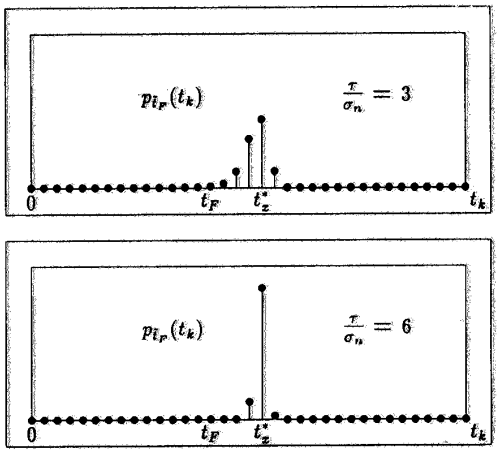

Figure 4. Probability mass function.

time-varying mean is equal to $a_o(t_k - t_F)^2$. The conditional probability density function $p(s_k|a_o, t_F)$ is

$$p(s_k|a_o, t_F) = \begin{cases} \frac{1}{\sqrt{2\pi}\sigma_n} \exp\left[-\frac{(s_k-\xi)^2}{2\sigma_n^2}\right] & \text{for } t_k \le t_F \\ \frac{1}{\sqrt{2\pi}\sigma_n} \exp\left[-\frac{[s_k - a_o(t_k-t_F)^2]^2}{2\sigma_n^2}\right] & \text{for } t_k > t_F \end{cases}$$

The probability mass function $p_{\tilde{t}_F}(t_k)$ for the noisy signal to exceed the threshold *first* at time sample t_k is

$$p_{\tilde{t}_F}(t_k) = \text{Prob}\{s_k < \tau \text{ for } t < t_k \text{ and } s_k \ge \tau \text{ for } t = t_k\}$$

Assuming independent noise samples n_k,

$$\begin{aligned} p_{\tilde{t}_F}(t_k) &= C_o \left[\prod_{j=0}^{k-1} \int_{-\infty}^{\tau} ds_j\, p(s_j|a_o, t_F)\right] \int_{\tau}^{\infty} ds_k\, p(s_k|a_o, t_F) \\ &= C_o \left[\prod_{j=0}^{k-1} \text{erf}_*(x_j)\right] [1 - \text{erf}_*(x_k)] \end{aligned} \tag{7}$$

where $$\text{erf}_*(x_i) \triangleq \frac{1}{\sqrt{2\pi}} \int_{-\infty}^{x_i} dy\, e^{-\frac{y^2}{2}},$$

$$x_i = \begin{cases} \frac{\tau - \xi}{\sigma_n} & \text{for } t_i \le t_F \\ \frac{\tau}{\sigma_n}\left[1 - \frac{(t_i - t_F)^2}{(t_z^* - t_F)^2}\right] & \text{for } t_i > t_F \end{cases}$$

and C_o is a normalization constant. The mass function $p_{\tilde{t}_F}(t_k)$ has been evaluated for values of $\tau/\sigma_n = 3, 6$ with the results shown in Fig. 4. For a particular obstacle, as τ/σ_n is increased by reducing σ_n and keeping τ constant, $p_{\tilde{t}_F}(t_k)$ approaches a Kronecker delta function located at $t_z^* + \Delta$: the mean crossover time approaches $t_z^* + \Delta$ and the estimator variance decreases. When considering the set of all obstacles, Δ becomes a random variable that is independent of t_z^*. Taking expectations over Δ, the variance of $\tilde{t}_F$ for large values of τ/σ_n approaches $T_s^2/12$. Since $E[\tilde{t}_F]$

becomes $t_x^* + \frac{T_s}{2}$, the bias takes the value,

$$B[\tilde{t}_F] = \sqrt{\frac{\tau}{a_o}} + \frac{T_s}{2} \tag{8}$$

The bias illustrates the problem inherent to thresholding: for $\tau > 0$, the true t_F occurs before the time t_x.

4.2 Parabolic Fit to the Signal Envelope

To reduce the bias, a parabola is fit to the signal envelope around its starting point t_F. Since the signal model of (5) is nonlinear in a_o and t_F, an explicit least squares solution for the unknown parameters is difficult to find. Instead, an iterative algorithm proposed by Marquardt [8] is employed. Suppose that N samples of the envelope fall within the time interval $[t_F,\ t_F + \frac{1}{2a_1}]$ where the parabolic model is valid. The algorithm starts with initial guesses for a_o and t_F and minimizes the sum of the squared errors between the signal samples and the model in (5), by employing a variable-step gradient method. Depending on the success of the trial parameters, the estimates $\hat{a}_o$ and $\hat{t}_F$ are updated, the gradient step size is varied and new trial values are generated. The algorithm terminates when the change in the TOF estimate is less than a preset value.

To compare the two methods of measuring TOF, an obstacle was placed at θ=0° and r=500mm, for which the true TOF is $t_F = \frac{2r}{c}$=2.91ms. The sampling rate is 50kHz, corresponding to a sampling interval T_s=20μs and τ was set equal to $6\sigma_n$. A pulse was transmitted and the TOF was estimated. 1000 trials were repeated to compute the mean and standard deviation of both estimators.

With the simple thresholding method, $E[\tilde{t}_F]$=3.00ms and $B[\tilde{t}_F]$=90μs or 4.5T_s. In this case, the range measurement is biased by 14.9mm. The standard deviation of the threshold crossover point is equal 8.28μs or 2.84mm. The analytical value predicted by Eq. (7) is 2.99mm which corresponds to the second case in Fig. 4. The standard deviation component due to sampling is 5.77μs or 1.98mm.

With the parabolic fit method, $E[\hat{t}_F]$=2.91ms. In this case, the estimator is unbiased but the standard deviation increased slightly to 9.30μs or 3.19mm. Hence, we have an unbiased estimate of range having a standard deviation comparable to thresholding.

5 Range and Azimuth Estimation

When the active region is occupied by an obstacle, two TOF measurements $\hat{t}_{F1}$ and $\hat{t}_{F2}$ are acquired from R1 and R2, corresponding to the distances $\hat{z}_1 = c\hat{t}_{F1}$ and $\hat{z}_2 = c\hat{t}_{F2}$ from the transmitter to each receiver. Measurement $\hat{z}_1$ restricts the possible locations for the obstacle to lie on an ellipse whose foci are at T and R1. Similarly, given $\hat{z}_2$, the possible obstacle locations lie on an ellipse with foci at T and R2, as shown in Fig. 5. Both measurements are valid only where the two ellipses intersect within the active region. From the geometry, the distances are given by

$$\begin{aligned} \hat{z}_1 &= \sqrt{r^2 + d^2 + 2dr\sin\theta} + r + e_1(r,\theta) \\ \hat{z}_2 &= \sqrt{r^2 + d^2 - 2dr\sin\theta} + r + e_2(r,\theta) \end{aligned} \tag{9}$$

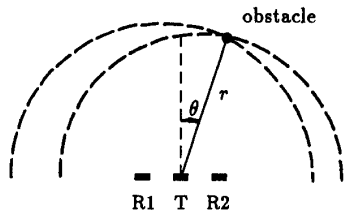

Figure 5. Geometry of obstacle localization.

where $e_1(r,\theta)$ and $e_2(r,\theta)$ are the zero-mean errors related to the error in the TOF estimate by the sonic speed c. Eq. (9) can be written in vector form as $\hat{\mathbf{z}} = \mathbf{f}(r,\theta) + \mathbf{e}(r,\theta)$. Since the error components at the two receivers are uncorrelated, $\mathbf{e}(r,\theta)$ is white Gaussian error with a diagonal covariance matrix $\mathbf{C}$. Therefore, the conditional probability density function of $\hat{\mathbf{z}}$ is:

$$p(\hat{\mathbf{z}}|r,\theta) = \frac{1}{2\pi \mid \mathbf{C} \mid} \exp\left\{-\frac{1}{2}[\hat{\mathbf{z}} - \mathbf{f}(r,\theta)]^T \mathbf{C}^{-1} [\hat{\mathbf{z}} - \mathbf{f}(r,\theta)]\right\}$$

The Maximum Likelihood Estimates of r and θ are:

$$\hat{r} = \frac{\hat{z}_1^2 + \hat{z}_2^2 - 2d^2}{2(\hat{z}_1 + \hat{z}_2)} \qquad \hat{\theta} = \sin^{-1}\left[\frac{(\hat{z}_1\hat{z}_2 + d^2)(\hat{z}_1 - \hat{z}_2)}{d(\hat{z}_1^2 + \hat{z}_2^2 - 2d^2)}\right]$$

6 Experimental Verification

A pole (1m height×25mm diameter) was placed at a set of known locations within the active region of the sonar system with d=120mm. A pulse was transmitted and $\tilde{t}_{F1}, \tilde{t}_{F2}$ and $\hat{t}_{F1}, \hat{t}_{F2}$ were computed. The range and azimuth were estimated by both methods of TOF estimation. For a given location, M=100 trials were conducted to compute the mean and the standard deviation of the estimates. The experiment was repeated for a collection of r and θ values.

7 Results and Interpretation

The results are shown in Figs. 6 and 7 where the solid-line curves represent the mean value of the estimate and the dashed and dotted lines correspond to the $\pm\sigma$ values. In Fig. 6, true r=500mm and θ varies between $-30°$ to $+30°$. The upper curve corresponds to the biased range estimate from the simple thresholding method whereas the lower curve is the range estimate from the parabolic fit method. The thresholding result indicates that $\tilde{r}$ is biased and that the bias increases with $|\theta|$. This result is expected from (8) because for obstacles located at large $|\theta|$, the signal amplitude decreases and the crossover occurs closer to the envelope maximum. This corresponds to smaller values for a_o and hence a larger bias by (8). The estimator $\hat{r}$ is observed to be essentially unbiased. The resulting $\tilde{\theta}$ in Fig. 7 is biased because at large $|\theta|$, the mean value deviates from the true value by more than three standard errors of the mean value given by $3\sigma_{\hat{\theta}}/\sqrt{M}$. For example, at θ=30°, $\tilde{\theta}$ equals 40.8°. ($3\sigma_{\hat{\theta}}/\sqrt{M}$=0.20°). This bias is mainly due to the biased TOF estimates used in (5). The result $\hat{\theta}$ is also slightly biased at large $|\theta|$. At θ=30°, $\hat{\theta}$ equals 32.3°.

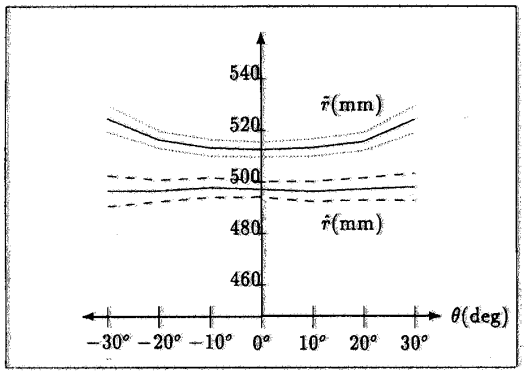

Figure 6. Comparison of the range estimators.

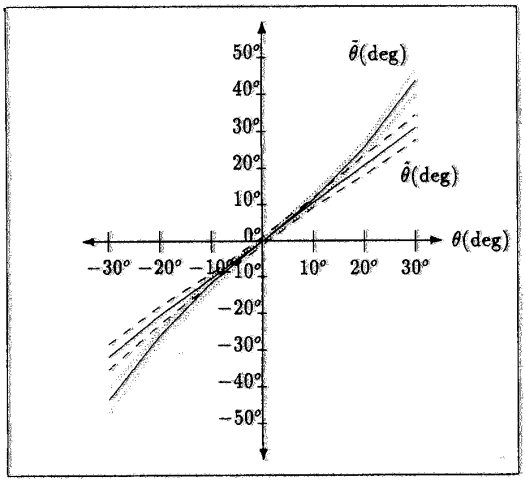

Figure 7. Comparison of the azimuth estimators.

($3\sigma_{\hat{\theta}}/\sqrt{M}$=0.22°). The estimate $\hat{\theta}$ is less biased than $\bar{\theta}$ because the TOF estimates with this method are unbiased. The small residual bias in $\hat{\theta}$ is due to the nonlinearity of the azimuth estimator.

Note that the standard deviation of each estimator is minimum at θ=0° and increases with $|\theta|$. The standard deviations of $\hat{\theta}$ and $\bar{\theta}$ also increase with range [9]. These results can be explained in terms of the transducer beam pattern given in (1), which indicates that the echo amplitude decreases with range and with increasing deviation $|\theta|$ from the transducer line-of-sight. Since the signal-to-noise ratio is smaller at larger deviations from the line-of-sight, the estimator variances are larger.

In the limit as $2d/r$ goes to zero, the behavior of the three transducer system resembles a single transducer system which can provide comparably accurate range estimates. These systems are, however, limited in their angular resolution, typically equal to $\pm\theta_o$. Angular localization is significantly improved with our three-transducer system.

As a measure of the parabolic fit estimator performance, Cramér-Rao lower bounds for estimator variances have been derived and compared to our experimental results in [9]. The bounds and the experimental results are of similar shape. At r=500mm and θ=0°, σ_t is comparable to the lower bound and $\sigma_{\hat{t}}$ is only 1.2 times larger. The lower bounds are not achieved by the experimental results because in estimating the TOF, a heuristic technique was used instead of the optimal correlation method [10]. Since the signal envelope parameters a_o and a_1 vary with range and azimuth, the optimal method requires the storage of a large number of reference signals. Our simple method gives an attractive compromise between accuracy and complexity.

8 Summary and Conclusions

We have described a three-transducer sonar system that demonstrates a significant improvement in object localization over the single transducer system. Simple thresholding does not produce accurate results due to the bias in the TOF measurement. With the parabolic fit method, TOF is extracted from the leading edge of the echo, eliminating the need for the whole pulse to be processed. The results provide useful insights about animal sonar systems. For successful capture of prey, it is crucial that the accuracy is best along the line-of-sight and at nearby ranges. This is exactly the type of behavior our system exhibits.

References

[1] J. L. Crowley. Navigation for an intelligent mobile robot. *IEEE J. Robotics Automation*, 1985.

[2] J. Borenstein and Y. Koren. Obstacle avoidance with ultrasonic sensors. *IEEE J.Robotics Automation*, 1988.

[3] A. Elfes. Sonar based real-world mapping and navigation. *IEEE J. Robotics Automation*, 3:249-265, 1987.

[4] R. Kuc and M. W. Siegel. Physically-based simulation model for acoustic sensor robot navigation. *IEEE J. PAMI*, 3:766-778, 1987.

[5] R. Kuc. A spatial sampling criterion for sonar obstacle detection. *IEEE J. PAMI*, 12:686-690, 1990.

[6] B. Barshan and R. Kuc. Differentiating sonar reflections from corners and planes by employing an intelligent sensor. *IEEE J. PAMI*, 12:560-569, 1990.

[7] Polaroid Corp. *Ultrasonic Components Group*, 1989.

[8] W. H. Press, B. P. Flannery, S. A. Teukolsky, W. T. Vetterling. *Numerical Recipes in Pascal*, pp. 574-579. Cambridge University Press, Cambridge, 1989.

[9] B. Barshan and R. Kuc. Sonar system for obstacle localization with insights from the echolocating bat. submitted to *IEEE Trans. Systems, Man, Cybernetics*.

[10] R. A. Altes. Angle estimation and binaural processing in animal echolocation. *JASA*, 63:155-173, 1978.